NANO LETTERS

Letter

pubs.acs.org/NanoLett

Ultrafast Electron and Phonon Response of Oriented and Diameter-Controlled Germanium Nanowire Arrays

Yanying Li,[†,∥] Raphael Clady,[‡,∥] Junghyun Park,[§] Shruti V. Thombare,[§] Timothy W. Schmidt,[‡] Mark L. Brongersma,[§] and Paul C. McIntyre*[,§]

[†]Department of Applied Physics and [§]Department of Materials Science and Engineering, Stanford University, Stanford, California 94305, United States

[‡]School of Chemistry, University of Sydney, Sydney, NSW 2006, Australia

Supporting Information

ABSTRACT: Carrier and phonon dynamics in dense arrays of aligned, single-crystal Ge nanowires (NWs) of controlled diameter are investigated by ultrafast optical pump−probe measurements, effective medium calculations, and elasticity analysis. Both a pronounced induced absorption and the amplitude and spectral range of Fabry−Perot oscillations observed in the probe signal are predicted for the NW array/air metamaterial by effective medium calculations. Detected temporal oscillations of reflectivity are consistent with excitation of radial breathing mode acoustic phonons by the intense pump pulse.

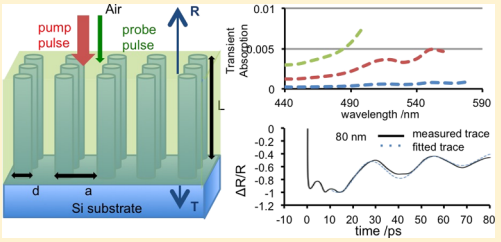

KEYWORDS: *Nanowire, ultrafast, absorption, phonon, metamaterial*

Semiconductor nanowires (NWs) have been investigated intensively in recent years due to the unique properties emerging from their anisotropic geometry, large surface-to-volume ratio, and ability to confine electronic carriers. The dynamics of electrons, photons, and phonons in NW assemblies strongly depend on such geometrical factors.[1] A better understanding of the fundamental photonic and acoustic properties of semiconductor NW assemblies is essential in order to exploit them in the design of nanoscale optoelectronic and thermoelectric devices.[2−9] However, investigations of ultrafast dynamics in semiconductor NWs are limited and have mainly focused on a small group of materials.[10−14]

In this work, we report on ultrafast, optical pump−probe measurements on dense arrays of single-crystal and relatively uniform-diameter Ge NWs on a silicon substrate. It was found that several coexisting physical phenomena govern the spectral and temporal dependence of the detected probe signal. These include intraband transitions that induce absorption, state-filling processes that ultimately limit this absorption and excitation of acoustic phonons by the intense pump laser pulse.

As the Ge NW array is dense, with many wires in a square (illumination) wavelength, it can be viewed as an anisotropic metamaterial layer with effective optical properties that can be extracted from an effective medium model. This model predicts the magnitude and free spectral range of Fabry−Perot oscillations seen in spectral reflectance data. Finally, the excitation of acoustic phonons in the NWs produces temporal oscillations in the reflection traces. Based on linear elasticity theory, the oscillations were attributed to excitation of the fundamental and overtone breathing modes of the Ge NWs. The temporal oscillations in the reflection traces were largely determined by two physical parameters: an acoustic damping time and oscillation period. Both parameters were observed to depend on the NW diameter, in good quantitative agreement with the theoretical analysis.

Undoped Si (111) substrates (N-type, resistivity >1000 ohm·cm), obtained from MTI Wafers, were used for the NW growth experiments. Si wafers were first dipped into freshly prepared piranha (9:1 H_2SO_4:30% solution of H_2O_2(aq)) to remove organic surface contaminants and then thoroughly rinsed in deionized water (DI water). They were then dipped in a 1:1:5 30% HCl(aq):30% H_2O_2(aq):water solution to remove metallic impurities, followed by DI water rinse. Si wafers were then dipped in 2% dilute HF for oxide removal. Commercially available 20, 40, and 80 nm diameter Au colloids, obtained from Ted Pella, Inc., were diluted in 2% HF with 10:1 colloid solution to HF ratio. The solutions were drop-cast on Si (111) substrates for 10 min. The samples were then dried with flowing nitrogen. Single-crystal Si (111) substrates, their surfaces decorated with colloidal Au nanoparticles, were transferred to the load-lock of a cold-walled CVD chamber for NW growth. The lamp-heated, CVD system used for the NW growth experiments has been described in a previous publication by Jagannathan et al.[15] A two-temperature growth procedure, which was previously developed for the epitaxial growth of untapered Ge NWs using gold as a catalyst,[16] was employed. The samples were heated up to 365 °C and held there for 90 s in the presence of GeH_4 diluted with H_2. The subsequent growth step temperature was 300 °C, with a

Received: March 13, 2014
Revised: April 21, 2014
Published: May 5, 2014

duration of 60 min to produce wires of ~7 μm length. Total pressure inside the reactor chamber was 30 Torr, with GeH_4 partial pressure of 0.75 Torr. The diameters of Ge NWs are mainly determined by, and slightly larger than, the diameters of the Au catalysts due to Au particles coarsening prior to wire nucleation. Figure 1a shows a representative SEM image of the vertically aligned, dense Ge NWs under investigation.

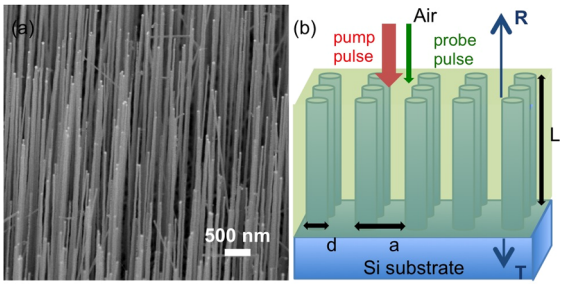

Figure 1. (a) SEM image of vertically aligned Ge NWs grown on a Si (111) substrate using 40 nm Au colloids. (b) Schematic of an idealized Ge NW array used to simulate the optical response, where the Ge NW array forms an effective medium slab.

A schematic of the oriented nanowire assembly and of the pump–probe process is shown in Figure 1b. A pump pulse excites the Ge NW array with illumination at near normal incidence. Then the photoexcited Ge NW array is measured by a probe pulse at near normal incidence, and the reflected probe signal is detected. Ultrafast pump–probe experiments use a Ti:sapphire oscillator-regenerative amplifier system producing a train of pulses (780 nm, 1 kHz, 1.5 mJ, and 150 fs per pulse, Clark MXR). The output beam is split into two equal parts to concurrently pump two optical parametric amplifiers (TOPAS-C, Light Conversion). The visible-OPA produces signal and idler beams, which are tunable from 1020 to 2600 nm. Two successive nonlinear crystals (LBO) allow for second and fourth harmonic generation of the amplified signal and idler as well as sum frequency mixing with the remaining portion of the pump pulse (780 nm). This system configuration provides 150 fs pulses with tunable wavelength over a range from 256 nm (4.84 eV) to 2.6 μm (0.48 eV). The deep-UV-OPA uses a similar optical arrangement to produce an independently tunable beam over a wavelength range from 187 nm (6.6 eV) to 2.6 μm (0.48 eV) and is used to generate the excitation pulse (pump). In the experiments described here, the pump wavelength was 780 nm (1.59 eV) for pulse duration around 230 fs, determined by autocorrelation. Similar pulse durations have been found for the different probe wavelengths we have used in this study.

All experiments were performed at room temperature with vertically polarized pump and probe, near normal incidence. The probe is detected after reflection from the sample substrate by a homemade integrating photodiode, coupled to a fast data acquisition card. A mechanical chopper, inserted in the pump line, is operated at half the laser repetition rate (500 Hz) and allows a pump-on pump-off configuration to determine the change in reflection coefficient induced by the pump pulse. As the reflection of the probe pulse occurs mainly at the Si substrate, the NWs are effectively measured in transmission.[17]

The diagram in Figure 2a illustrates various related processes occurring in photoexcited semiconductors.[18] Electrons are excited into the conduction band after the pump pulse and then

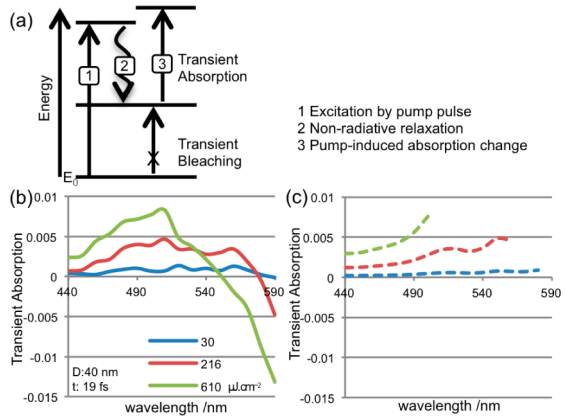

Figure 2. (a) Schematic of TA and transient bleaching phenomena and related processes in photoexcited semiconductors. (b) Differential absorption spectra of Ge NWs grown with Au catalysts of 40 nm diameter for different pump fluences at 19 fs after the pumping pulse. The vertical axis of the absorption spectra is defined as $\log(1 - \text{reflected signal/reference})_{\text{with pump}} - \log(1 - \text{reflected signal/reference})_{\text{without pump}}$, where reference is the signal on the photodiode reflected by the beam splitter (not incident on the sample). (c) Simulated differential absorption spectra immediately after pumping for different levels of pump fluence. Simulated spectra in the wavelength range where state-filling effect dominates are not shown.

relax to the band edge within a few picoseconds. When a probe pulse arrives, two phenomena may occur. One is the prohibition of the excitation of electrons from valence band to conduction band, because the final states have already been occupied by excited electrons. This leads to a decrease of absorption, showing a transient bleaching in the spectra. Similar bleaching of interband optical transitions has previously been reported in semiconductor nanocrystals,[19−24] single semiconductor NWs,[11,18] and ensembles of semiconductor NWs.[14,17,25] The other phenomenon that occurs during absorption of the probe pulse is the further excitation of electrons already in the conduction band, from states near the band edge to available higher energy states. This leads to an increase of absorption.[18,26] Figure 2b shows our measured transient absorption (TA) spectra for different pump fluences incident on a Ge NW array. This plot indicates the coexistence of two competing physical phenomena governing the spectra. Transient bleaching, which dominates for probe wavelengths around 600 nm, reduces absorption, whereas TA, prominent in the shorter probe wavelength range, enhances it.

The measured spectra also indicate that, at high pump fluence, where more free carriers are generated in the NWs, the absolute value of induced absorption is larger.[26] On the other hand, in the probe wavelength range of 560–590 nm, the state-filling effect limits the induced absorption, and for longer probe wavelengths, it leads to a decrease of absorption and becomes more prominent as pump fluence increases. This is evidenced by both the increasing scale (about 10 times) and the blue-shift of the differential absorption edge. This result demonstrates the impact of state filling in the Ge conduction band on optical absorption by the nanowires: The pump pulse produces filled states in the L-valley of the Ge conduction band,[27,28] and therefore, probe photons with energy just above the energy gap, which would be absorbed without the prior pump pulse, are absorbed at a much lower rate. Higher pump fluence produces more filled states,[19] and therefore the effect described above is stronger, producing both an increase in the range of probe

dx.doi.org/10.1021/nl500953p | Nano Lett. 2014, 14, 3427−3431

wavelengths which show reduced absorption and a greater overall reduction in absorption shown in Figure 2b. The absorption edge in Figure 2b shifts from 590 to 550 nm with increasing pump fluence, which is consistent with the fact that the empty L-valley has a direct energy gap of 2.1 eV.[29]

Different from previous reports,[17] Fabry–Perot oscillations were also observed in the TA spectra of Ge NW arrays, which arise from the interference produced by the reflected and transmitted probe light. The observed Fabry–Perot oscillations suggest the vertical NW assemblies investigated here have relatively uniform dimensions and behave as a slab of uniform meta-material responding to the incident light in the studied probe wavelength range.

There are few reports of free carrier absorption in photoexcited semiconductor NW arrays. Therefore, to better understand this TA, we combined several models to simulate the process. First of all, because the diameters of NW's are much smaller than the wavelengths of incident light, we assume the Ge NW arrays behave as a slab of uniform meta-material with an effective refractive index. Based on the effective media model, we use an idealized NW assembly, as shown in Figure 1b to calculate the effective refractive index of actual Ge NW array samples. Nanowires with diameter d are arranged in a square lattice of period a in both x and y directions and have a length L in the z direction. A circularly polarized light is incident on this structure with an incident angle θ. The filling ratio of the Ge NW array/air medium is given by

$$f_s = \pi(d/2)^2/a^2 \tag{1}$$

In the following, we focus on a structure with a filling ratio f_s = 0.07 (d = 40 nm, a = 135 nm) and L = 7 μm. The Ge NW array can be viewed as an effective medium with an effective dielectric constant given by[30]

$$\frac{\varepsilon_x - \varepsilon_2}{\varepsilon_x + \varepsilon_2} = \frac{\varepsilon_1 - \varepsilon_2}{\varepsilon_1 + \varepsilon_2} f_1 \tag{2}$$

Here $\varepsilon_1 = \varepsilon_{Ge}$,[31] $\varepsilon_2 = 1$, and $f_1 = f_s$, the filling ratio of eq 1. This model gives an effective complex refractive index $n_e = (\varepsilon_x)^{1/2}$ = 1.069 + 0.003i of Ge NW array for a wavelength of 550 nm prior to excitation by the pump pulse.

Following photoexcitation by the pump pulse, the refractive index of Ge changes with free carrier concentration, which should be accounted for in the effective medium model. The change in the real part of the index (Δn) and in the imaginary part of index (Δk) produced by a nonequilibrium concentration of electrons (ΔN) and a nonequilibrium concentration of holes (ΔP) can be estimated using the Drude model:[32]

$$\Delta n = \frac{-e^2\lambda^2}{8\pi^2 c^2 \varepsilon_0 n}\left(\frac{\Delta N}{m_{ce}^*} + \frac{\Delta P}{m_{ch}^*}\right) \tag{3}$$

$$\Delta k = \frac{e^3\lambda^3}{16\pi^3 c^3 \varepsilon_0 n}\left(\frac{\Delta N}{\mu_e (m_{ce}^*)^2} + \frac{\Delta P}{\mu_h (m_{ch}^*)^2}\right) \tag{4}$$

where e is the electron charge, λ is the optical wavelength, c is the speed of light, ε_0 = 8.85 × 10^{-12} F·m^{-1}, n is the initial refractive index at λ, m_{ce}^* and m_{ch}^* are the conductivity effective masses, and μ_e and μ_h are the electron and hole mobilities at carrier concentrations ΔN and ΔP. Referring to published data,[33] the masses and mobilities for Ge are listed in Table 1. As suggested in the Drude model, the imaginary part of k, proportional to the absorption coefficient, increases with carrier concentration. Therefore, we should expect transient-induced absorption due to free carriers excited by the pump pulse.

Table 1. Effective Mass and Mobility for Ge[a]

m_{ep} (m_0)	0.0807
m_{et} (m_0)	1.57
m_{hl} (m_0)	0.0438
m_{hh} (m_0)	0.284
m_{ce}^* (m_0)	0.118
m_{ch}^* (m_0)	0.0759
μ_e at 10^{18}cm^{-3} (cm^2 V^{-1} s^{-1})	900
μ_h at 10^{18}cm^{-3} (cm^2 V^{-1} s^{-1})	470

[a]See refs 32 and 33.

To further model the induced absorption in Ge NWs, we use the transfer matrix method (TMM), considering a layered structure: air, Ge NW/air meta-material, Si substrate. More details can be found in the Supporting Information.

Combining these three models, TA spectra at various times after the pump and at different levels of pump power can be simulated, as shown in Figure 2c. Here we assume with a carrier density of 5 × 10^{19} cm^{-3} at a pump fluence 30 μJ/cm^2,[17] that the photoexcited carrier density of the sample increases linearly with pump fluence. The cutoff of the simulated spectra in Figure 2c occurs because the modeling focuses on free carrier absorption, but for longer probe wavelengths, the measured spectra are dominated by the bleaching process. Comparing the simulated induced absorption to the measured spectra indicates a reasonable fitting of the TA intensity for different levels of pump fluence. The simulated spectra also show Fabry–Perot oscillations, which demonstrates that these effects are captured reasonably well with the effective medium and free carrier models.

For probe wavelengths in the range dominated by induced absorption, besides the significant initial absorption, subsequent temporal oscillations are also observed in differential reflection traces. These oscillations result from the transient excitation of acoustic phonons in the Ge NWs after exposure to the intense pump pulse. Temporal changes in NW absorption via acoustic vibrational modes occur due to both shape changes of the vibrating NWs and an oscillating strain-induced change of the band gap,[34] resulting from photoelasticity.[13] Breathing modes have also been investigated by ultrafast TA measurement in both ensemble and individual particle studies of metal[35−37] and semiconductor NWs.[10−13,38,39] We measured differential reflection traces for Ge NW arrays grown with Au catalysts of 20, 40, and 80 nm diameter. For each case, the probe wavelength is chosen to be in the range producing induced absorption. A representative reflection trace of the 80 nm samples is shown in Figure 3a. In addition to the exponential decay background, the trace also shows oscillations with well-defined periods and the damping of these oscillations with increasing time after the pump pulse.

The frequencies of the radial breathing modes and axial modes for a solid cylinder can be estimated using linear elasticity theory.[35] In this report, we focus only on the radial breathing modes, because the period of the fundamental axial extension mode calculated from linear elasticity theory is about 4 ns for the Ge NW arrays under study,[35] longer than the time window of the current experiment. For a long isotropic cylinder, in the limiting case of $L/d \gg 1$, where L is the NW length and d is its diameter, the frequency of such a radial breathing mode is given by[35]

dx.doi.org/10.1021/nl500953p | Nano Lett. 2014, 14, 3427−3431

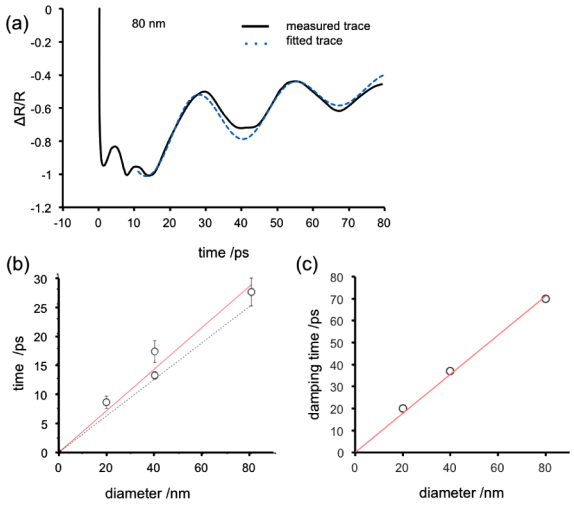

Figure 3. (a) Solid line: optical differential reflection traces for Ge NWs grown with Au catalysts of 80 nm diameter. The pump wavelength was 780 nm, and the probe wavelength was 550 nm. Dashed line: Damped cosine function with an exponentially increasing background fitted to the measured trace. (b) Plots of the measured breathing mode period versus Au catalyst diameter. The error bar represents the standard deviation of vibrational period for each sample. Periods were evaluated from reflection data collected with probe wavelength in the regime in which induced absorption is strong for each sample. The solid line is a fit to the data. The dotted line displays the theoretically predicted trend. (c) Damping time of fitted differential reflection traces for NWs grown with different diameter Au catalysts.

$$f_n = \frac{x_n}{\pi d}\sqrt{\frac{E(1-\nu)}{\rho(1+\nu)(1-2\nu)}} \tag{5}$$

where E and ν are, respectively, the Young's modulus and the Poisson ratio of Ge. The parameter x_n is the n^{th} nontrivial root of

$$xJ_0(x) - \frac{(1-2\nu)}{(1-\nu)}J_1(x) \tag{6}$$

where $J_m(x)$ is the m^{th} Bessel function of the first kind.[35] For Ge, E = 103 GPa, ν = 0.26, and the density, ρ = 5323 kg/m^3.[40] Numerical solution of eq 6 yields x_1 = 2.08 and x_2 = 5.40, corresponding to the fundamental breathing mode and the overtone breathing mode, respectively. Using these parameters, an expression for the oscillation period of the fundamental breathing mode is given by

$$\tau = Cd \tag{7}$$

where C = 0.310 ps/nm.

Figure 3b displays the relationship between the measured fundamental breathing mode period and Au catalyst diameter. The observed periods of vibration are consistent with the fundamental breathing mode simulation using bulk elastic parameters (C = 0.310 ps/nm, dotted line). Assuming NW diameters equal to their Au catalyst diameters, a fit to the data (solid line) yields C = 0.353 ± 0.018 ps/nm (1σ), which agrees with the experimental results at the 3σ level of confidence. The larger fitted C value can be partly explained by the underestimation of the NW diameters due to Au particles coarsening prior to wire nucleation. An earlier report from our group has shown that Ge NWs prepared and grown under the same conditions used in this study and with 40 nm diameter Au colloid catalysts have a diameter distribution of 59.15 ± 5.36 nm (1σ).[41] The slight difference shown in Figure 3b can also be traced back to an assumption of the linear elasticity theory model: In the theoretical calculation, the material is assumed to be elastically isotropic, which is not true for single crystal NWs.

A further analysis of the fundamental breathing mode signals can be performed using a general fitting function for the traces:

$$\Delta R/R = M_1\exp(-t/\tau_1) + M_2\cos(2\pi t/\tau_3 + \phi)\exp(-t^2/\tau_2{}^2) \tag{8}$$

where τ_1 is the time constant of the induced absorption, τ_2 is the damping time of the breathing mode oscillations, τ_3 is the period of the oscillations, M_1 and M_2 are constant coefficients, and ϕ is a fitting phase shift. Here an $\exp(-t^2/\tau_2{}^2)$ damping term is chosen based on the assumption that the damping of the oscillations is dominated by dephasing due to the diameter variation of the NWs.[35,42] An alternative mechanism to damping is the energy relaxation to the environment, which corresponds to an exponential damping term.[43−45] Our measurement and analysis show that the fitted damping time is too short to be consistent with energy relaxation to the environment. The dashed line in Figure 3a is a fitting function profile to the measured trace for the 80 nm samples. Fitted values of time constants and coefficients are shown in Table 2.

Table 2. Fitted Constants of Reflection Profile in Figure 3a

constants	M_1	M_2	τ_1
values	0.9	0.22	115
constants	τ_2	τ_3	ϕ
values	70	27.3	−0.08

Figure 3c plots the damping time versus Au catalyst diameter, and a linear regression is performed on the data. Within a small error range, one can see that the damping time τ_2 increases linearly with diameter. The damping time due to the size distribution can be estimated by[42]

$$\tau_2 = \frac{\overline{dT}}{\sqrt{2}\,\pi\sigma_d} \tag{9}$$

where $\overline{d}$ is the mean diameter of the sample, σ_d is the standard deviation, and $\overline{T}$ is the mean period of modulation. A theoretical damping time for Ge NWs grown with 40 nm diameter Au colloids can be estimated using formula 9 and $\overline{d}$ = 59.15 ± 5.36 nm,[41] which yields a value of 35.1 ps, close to the fitted value of 37 ps as shown in Figure 3c. In addition, we have shown above that the period of modulation is linearly increasing with the diameter of NWs, therefore formula 9 can be rewritten as

$$\tau_2 = \frac{C}{\sqrt{2}\,\pi}\overline{d}/\frac{\sigma_d}{\overline{d}} \tag{10}$$

where the term $\sigma_d/\overline{d}$ is normalized standard deviation by mean diameter, which can be considered as a metric of size distribution. The linear relation between τ_2 and d shown in Figure 3c indicates that the size distribution varies slightly for Ge NWs grown with Au particles of different diameters.

It is interesting to note that both fundamental and overtone breathing modes are observed, as shown in Figure 3a. The fast component shown in the signal has an oscillation period of about 7 ps for the 80 nm samples, close to the theoretical overtone breathing period from eq 5, which is 9.5 ps. Thus, the

dx.doi.org/10.1021/nl500953p | Nano Lett. 2014, 14, 3427−3431

fast oscillating component is assigned to the overtone (second-order) breathing mode.[11,35] The fitting of the overtone breathing mode in differential reflection traces is difficult because of several poorly understood transitions involved in this time window.[11,27] Note that the amplitude of the fundamental mode is larger than that of the overtone mode and that the strong coupling of the overtone mode to the probe transition observed in single CdTe NWs[11] is not observed in our experiment.

In conclusion, we have shown by ultrafast pump−probe spectroscopy that the response of photoexcited vertical Ge NW arrays includes two competing effects governing the spectral and temporal dependence of the detected probe signal: induced absorption and state-filling bleach. Simulations that combine an effective medium model, the Drude model, and the transfer matrix method enable the quantitative determination of pump-induced carrier concentrations and relaxation processes. In addition, the acoustic phonon response, including both fundamental and overtone breathing modes, has been investigated using linear elasticity theory. The uniform dimensions of Ge NW arrays allow quantitative analysis of the measured temporal oscillations in reflection traces. Both oscillation period and damping time were measured as functions of Ge NW diameter and are in good quantitative agreement with a theoretical analysis of the effects of intense pump illumination on acoustic phonons in these nanostructures. The detected vibrational response is a probe of electron−phonon interaction in photoexcited Ge NWs and of energy relaxation mechanisms in these nanoscale semiconductor crystals.

■ ASSOCIATED CONTENT

Supporting Information

Transfer matrix method (TMM), considering a layered structure: air, Ge NW/air meta-material, Si substrate details. This material is available free of charge via the Internet at http://pubs.acs.org.

■ AUTHOR INFORMATION

Corresponding Author

*E-mail: pcm1@stanford.edu

Author Contributions

‖These authors contributed equally.

Notes

The authors declare no competing financial interest.

■ ACKNOWLEDGMENTS

We acknowledge the financial support of the National Science Foundation (DMR 1206511).

■ REFERENCES

(1) Hochbaum, A. I.; Yang, P. *Int. Nanoelectron. Conf., 3rd* **2010**, *110*, 527−546.
(2) Das, A.; Heo, J.; Jankowski, M.; Guo, W.; Zhang, L.; Deng, H.; Bhattacharya, P. *Phys. Rev. Lett.* **2011**, *107*, 066405.
(3) Xiao, Y.; Meng, C.; Wang, P.; Ye, Y.; Yu, H.; Wang, S.; Gu, F.; Dai, L.; Tong, L. *Nano Lett.* **2011**, *11*, 1122−1126.
(4) Yu, S.; Witzigmann, B. *Opt. Express* **2013**, *21* (Suppl1), A167−72.
(5) Kempa, T. J.; Tian, B.; Kim, D. R.; Hu, J.; Zheng, X.; Lieber, C. M. *Nano Lett.* **2008**, *8*, 3456−3460.
(6) Tian, B.; Zheng, X.; Kempa, T. J.; Fang, Y.; Yu, N.; Yu, G.; Huang, J.; Lieber, C. M. *Nature* **2007**, *449*, 885−889.
(7) Garnett, E. C.; Yang, P. *J. Am. Chem. Soc.* **2008**, *130*, 9224−9225.
(8) Yang, Y. T.; Callegari, C.; Feng, X. L.; Ekinci, K. L.; Roukes, M. L. *Nano Lett.* **2006**, *6*, 583−586.
(9) Li, M.; Tang, H. X.; Roukes, M. L. *Nat. Nanotechnol.* **2007**, *2*, 114−120.
(10) Kolomenskii, A. A.; Jerebtsov, S. N.; Liu, H.; Zhang, H.; Ye, Z.; Luo, Z.; Wu, W.; Schuessler, H. A. *J. Appl. Phys.* **2008**, *104*, 103110.
(11) Lo, S. S.; Major, T. A.; Petchsang, N.; Huang, L.; Kuno, M. K.; Hartland, G. V. *ACS Nano* **2012**, *6*, 5274−5282.
(12) Mariager, S. O.; Khakhulin, D.; Lemke, H. T.; Kjaer, K. S.; Guerin, L.; Nuccio, L.; Sørensen, C. B.; Nielsen, M. M.; Feidenhans'l, R. *Nano Lett.* **2010**, *10*, 2461−2465.
(13) Sakuma, H.; Tomoda, M.; Otsuka, P. H.; Matsuda, O.; Wright, O. B.; Fukui, T.; Tomioka, K.; Veres, I. a. *Appl. Phys. Lett.* **2012**, *100*, 131902.
(14) Prasankumar, R. P.; Upadhya, P. C.; Taylor, A. J. *Phys. Status Solidi* **2009**, *246*, 1973−1995.
(15) Jagannathan, H.; Deal, M.; Nishi, Y.; Woodruff, J.; Chidsey, C. E. D.; McIntyre, P. C. *J. Appl. Phys.* **2006**, *100*, 024318.
(16) Adhikari, H.; Marshall, A. F.; Chidsey, C. E. D.; McIntyre, P. C. *Nano Lett.* **2006**, *6*, 318−323.
(17) Prasankumar, R. P.; Choi, S.; Trugman, S. a; Picraux, S. T.; Taylor, a J. *Nano Lett.* **2008**, *8*, 1619−1624.
(18) Lo, S. S.; Devadas, M. S.; Major, T. A.; Hartland, G. V. *Analyst* **2013**, *138*, 25−31.
(19) Klimov, V. I. *J. Phys. Chem. B* **2000**, *104*, 6112−6123.
(20) Klimov, V.; Schwarz, C.; McBranch, D.; Leatherdale, C.; Bawendi, M. *Phys. Rev. B* **1999**, *60*, R2177−R2180.
(21) Kambhampati, P. *Acc. Chem. Res.* **2011**, *44*, 1−13.
(22) Kambhampati, P. *J. Phys. Chem. C* **2011**, *115*, 22089−22109.
(23) Huang, J.; Stockwell, D.; Huang, Z.; Mohler, D. L.; Lian, T. *J. Am. Chem. Soc.* **2008**, *130*, 5632−5633.
(24) Knowles, K. E.; McArthur, E. A.; Weiss, E. A. *ACS Nano* **2011**, *5*, 2026−2035.
(25) Ahn, H.; Yu, C.-C.; Yu, P.; Tang, J.; Hong, Y.-L.; Gwo, S. *Opt. Express* **2012**, *20*, 769.
(26) Song, J. K.; Willer, U.; Szarko, J. M.; Leone, S. R.; Li, S.; Zhao, Y. *J. Phys. Chem. C* **2008**, *112*, 1679−1684.
(27) Bailey, D. W.; Stanton, C. J. 1995, 2107.
(28) Othonos, A. *J. Appl. Phys.* **1998**, *83*, 1789.
(29) Cohen, M.; Bergstresser, T. *Phys. Rev.* **1966**, *141*, 789−796.
(30) Xiong, Z.; Zhao, F.; Yang, J.; Hu, X. *Appl. Phys. Lett.* **2010**, *96*, 181903.
(31) Aspnes, D.; Studna, A. *Phys. Rev. B* **1983**, *27*, 985−1009.
(32) Soref, R. A.; Friedman, L. *Int. J. Optoelectron.* **1994**, *9*, 205−210.
(33) Madelung, O. *Semiconductors: Group IW elements and III-V Compounds*; Springer-Verlag: Berlin, 1991; pp 5−57.
(34) Liu, J.; Sun, X.; Pan, D.; Wang, X.; Kimerling, L. C.; Koch, T. L.; Michel, J. *Opt. Express* **2007**, *15*, 11272−11277.
(35) Hu, M.; Wang, X.; Hartland, G. V.; Mulvaney, P.; Juste, J. P.; Sader, J. E. *J. Am. Chem. Soc.* **2003**, *125*, 14925−14933.
(36) Sando, G. M.; Berry, A. D.; Owrutsky, J. C. *J. Chem. Phys.* **2007**, *127*, 074705.
(37) Staleva, H.; Hartland, G. V. *Adv. Funct. Mater.* **2008**, *18*, 3809−3817.
(38) Chen, H.-P.; Wu, Y.-C.; Sheu, J.-K.; Sun, C.-K. *IEEE* **2011**, 1−2.
(39) Carey, C. R.; Yu, Y.; Kuno, M.; Hartland, G. V. *J. Phys. Chem. C* **2009**, *113*, 19077−19081.
(40) *Handbook series on semiconductor parameters*; Levinshtein, M.; Rumyantsev, S.; Shur, M., Eds.; World Scientific, Singapore, 1996.
(41) Koto, M.; Marshall, A. F.; Goldthorpe, I. a; McIntyre, P. C. *Small* **2010**, *6*, 1032−1037.
(42) Hartland, G. V. *J. Chem. Phys.* **2002**, *116*, 8048−8055.
(43) Nelet, A.; Crut, A.; Arbouet, A.; Del Fatti, N.; Vallée, F.; Portalès, H.; Saviot, L.; Duval, E. *Appl. Surf. Sci.* **2004**, *226*, 209−215.
(44) Pelton, M.; Sader, J. E.; Burgin, J.; Liu, M.; Guyot-Sionnest, P.; Gosztola, D. *Nat. Nanotechnol.* **2009**, *4*, 492−495.
(45) Voisin, C.; Del Fatti, N.; Christofilos, D.; Vallée, F. *Appl. Surf. Sci.* **2000**, *164*, 131−139.